Journal of Materials Chemistry B

Accepted Manuscript

ROYAL SOCIETY OF CHEMISTRY

www.rsc.org/materialsB

Journal of

Materials Chemistry B

RSC Publishing

PAPER

A Novel Pseudo-Protein-based Biodegradable Coating for Magnesium Substrate: In vitro corrosion phenomena and cytocompatibility

Cite this: DOI: 10.1039/x0xx00000x

J. Liu[a], X.L. Liu[b], T.F. Xi[a,c,]*, C.C. Chu[d],

The goal of this study is to examine whether a member of the newly developed biodegradable pseudo-protein biomaterial family could provide a far better protection and performance than the popular hydrolytically degradable poly (glycolide-co-lactide) (PLGA) biomaterial on an experimental magnesium substrates as a model. A member of the phenylalanine-based poly (ester amide)s (8-Phe-4) was chosen as a model pseudo-protein polymer to coat onto as-cast magnesium (Mg) metal as the experiment model. The microstructures of the coatings were characterized by SEM, FTIR and water contact angle. Nano-scratch test data indicated the scratch resistance and elastic resilience of the 8-Phe-4 coating were superior to PLGA coating. Standard electrochemical measurements along with the long-term immersion results indicated that the 8-Phe-4 coating had preferable in vitro degradation and corrosion behavior than the PLGA-coated Mg. Cytocompatibility was conducted via vascular smooth muscle cells (VSMC) and human umbilical vein endothelial cells (ECV304), and the 8-Phe-4 coating showed significantly better cell viability than the pure Mg and PLGA-coated Mg substrates over a 3 day incubation period. The favorable anti-corrosion behavior and cytocompatibility of 8-Phe-4 coating suggest that the newly developed biodegradable pseudo-protein biomaterial family may have the great potential to enhance the protection and performance of the Mg-based biomaterials and their application over the popular PLGA as the biodegradable coating material, and may bring the application of the Mg-based biomaterials closer to clinical reality.

Received 00th January 2012,
Accepted 00th January 2012

DOI: 10.1039/x0xx00000x

www.rsc.org/

1. Introduction

Magnesium has recently been considered to be a potential biomaterial in biodegradable implants, such as metallic cardiovascular stents, bone fixation materials and scaffolds for bone repair; and the data reported have been promising[1, 2]. In the application of cardiovascular stents, those implants, which can degrade on demand *in vivo* following the completion of their intended functions, are beneficial because they can significantly lower the risk of long-term complications associated with permanent implants, including foreign-body induced inflammatory response, displacement and restenosis of the stent, late lumen loss, delayed type hypersensitivity, and painful secondary removal surgery[3, 4].

The most obvious challenge of those biodegradable Mg-based stents is their rather fast *in vivo* degradation rate, resulting in an early loss of the mechanical properties and following restenosis. Besides, magnesium alloys, such as WE43 can induce rather high hemolysis rate (9.27%) as well as cell toxicity[5], which illustrate the inadequacy of using bare magnesium alloy as biodegradable implants. Although tailing the microstructure and composition of the Mg-based stents through alloying[6], developing optimized manufacturing methods in addition to exploring suitable raw materials[7] are possible ways to improve the corrosion behaviour of Mg alloys, various surface coating and modification techniques have recently become more promising due to the relative simpler approach with reasonable good results.

Generally, coatings on metal surfaces can be divided into two categories: conversion coatings and deposited coatings[8]. Conversion coatings arise in a complex interaction of metal dissolution and precipitation[8], include anodization[9, 10], alkaline treatment[11], fluoride treatments[12-14], silanization[15-17]. In addition to wet chemical immersion methods, conversion coatings also produce oxidation processes by some dry methods using atmospheric[18-20] and temperature effects[21]. Deposited coatings include metallic coating[22], inorganic coating[23, 24] and organic coating[25-28]. For the case of cardiovascular stents applications, an ideal coating, besides providing corrosion resistance for alloy, should also possess additional functions, such as the enhancement of biocompatibility, having antibiotic ability, bioactivity and promoting endothelialization, as these functions are also desirable for facilitating wound

healing. Moreover, the coatings should be able to regulate biodegradation at a desired rate, and thus offering a limited barrier function[8] rather than totally prohibiting alloy biodegradation.

Among various polymeric coating for biodegradable implants, most research has focused on using existing commercially available absorbable aliphatic polyesters, for example polylactide (PLA)[29, 30] poly-ε-caprolactone (PCL)[31] poly (glycolic acid) (PGA)[32] and their lactide copolymer, PLGA. These aliphatic polyesters undergo bulk hydrolytic degradation mechanism, i.e., hydrolytic degradation proceeds throughout the whole biomaterial simultaneously. Among all these commercial aliphatic polyesters, Poly (lactic-co-glycolic acid) (PLGA) combines the advantages of mechanical strength together with processibility, and has become increasingly popular to coat Mg-based materials, such as magnesium alloy WE42[33], Mg-Zn[34, 35], as-forged Mg[36]. However, their broader applications in the biomedical field are limited because they cannot meet certain biological requirements because of their weak bonding to metallic substrates, poor mechanical strength, undesirable acidic degradation products[36, 37], and lack of functionality along the polyester chains. Particularly, the acidic environment with pronounced changes in pH upon PLGA hydrolytic bulk degradation could lead to a much faster corrosion of magnesium alloys than in the buffer solution like body fluid. Most importantly, its bulk degradation mechanism[37] leads to a rather quick erosion rate, thus limiting broader application of PLA and PGA derivatives, particularly in Mg-based stents.

Very recently, a new family of synthetic biodegradable polymers, amino acid based poly (ester amide)s (AA-PEA), have been investigated as a potential coating for drug-eluting stents[38-40], a scaffold for tissue-engineering purposes[41-45], as an efficient drug and gene delivery vehicle[46-48], and biologically active dressing for treating burns[49]. AA-PEA are synthesized from three naturally-occurring and non-toxic building blocks: amino acids, diacids and dialcohol[50, 51]. AA-PEAs have been widely studied in recent years because they combine the favourable properties of polyesters and polyamides; that is, they possess not only good biodegradability but also good mechanical and processing properties, such as modulus, thermal stability and tensile strength. In three reported *in vivo* porcine coronary artery and human trial studies using a Leu-based PEA as the coating for stainless steel and cobalt-based non-biodegradable stents[39, 40, 52], the elastomeric nature of the AA-PEA biomaterials provided a very smooth and complied coating without defects, cracks or delamination upon compression and expansion during stent delivery. These encouraging *in vivo* animal and human data suggest that AA-PEA biomaterials may have the potential to improve the performance of the biodegradable Mg-based alloys, particularly the protection against undesirable mode of corrosion and better biocompatibility toward cardiovascular tissues. Due to the biodegradation nature of Mg-based stents, it is expected that the coating for these biodegradable Mg-based biomaterials would be more demanding than the non-biodegradable Stainless steel and Co-based stents.

A variety of functional AA-PEAs have recently been reported[48, 50]. Their composition includes unsaturated diols and/or diacids[53-58] used to synthesize unsaturated AA-PEAs, using either polar amino acids like lysine (Lys), arginine (Arg), non-polar amino acids like phenylalanine (Phe), valine (Val), leucine (Leu) or an unsaturated >C=C< moiety in the backbone or pendant groups to provide pendant functionalized AA-PEAs[42-44, 46-48, 50, 51, 53, 54, 57, 59-64]and the different arrangement of these building blocks along the backbone[42, 53, 54, 60, 61, 65]. The inclusion of phenylalanine in the backbone of AA-PEAs can enhance their biodegradability with enzymes like chymotrypsin[53-55, 59]. The biodegradation mechanism of AA-PEAs is of surface erosion nature and mostly according to zero-order kinetics, but, their biodegradation rate in a pure saline buffer or simulated body fluid is slow (several months to years)[58, 66], thus providing an advantage of more stable and longer shelf-life than PGA, PLA and their copolymers, which are considered moisture sensitive, and hydrolytically degradable via bulk degradation.

The amino acid-based PEAs as a biodegradable drug-eluting coating on 316L stainless stents were investigated in an porcine model[39], and the 28 day implantation data suggest that under a dynamic coronary artery condition, these new biodegradable AA-PEA polymers are as biocompatible as bare stents with a similar level of inflammatory response as the bare stent[39]; An *in vitro* study of blood and cellular response to amino acid-based PEAs reported a much higher proliferation of endothelial cells on AA-PEA substrates than on non-biodegradable polymers, such as polyethylene vinyl acetate copolymer, poly (n-butyl methacrylate) or PCL[44, 64, 67]. In addition, AA-PEAs induced far less secretion of pro-inflammatory cytokines like interleukin (IL)-6, IL-1beta, and TNF-alpha by adhered monocytes or macrophage than PLGA or PCL polymers[44, 46, 47, 67]. These unique biological properties of AA-PEAs suggest their potential application as a new family of biodegradable biomaterials for metallic Mg-based biomaterials for cardiovascular stents coating, drug carriers or components of other absorbable surgical implants.

In the present study, the phenylalanine based poly (ester amide)s, 8-Phe-4, was chosen as an AA-PEA model compound to prepare protective films on the surface of the as-cast pure magnesium substrates as a model for a preliminary assessment of the feasibility to extend the observed merits of elastomeric AA-PEA coating on non-biodegradable stainless steel and Co-based stents to biodegradable Mg-based biomaterials. The study focused on the characterization of the Phe-based -PEA coating films including microstructure, hydrophilicity, nano-scratch resistance, *in vitro* degradation and corrosion behavior as well as *in vitro* cytocompatibility of the polymer-coated as-cast Mg. ASTM standard characterization methods as well as published methods were used in the current study. The data were compared with the poly (lactic-co-glycolic acid) (PLGA) coated Mg substrate for assessing the merits of the Phe-based-PEA coating. The data obtained will be used in a future comprehensive study using Mg stent model to validate the *in vitro* data obtained in the current study.

2. Materials and methods

2.1. Materials and samples preparation

As-cast pure magnesium was acquired from Hunan Research Institute of Nonferrous Metal (Hunan, China) and was used as received. Mg substrates were sliced from the Mg block into thin squares 10×10×1.2 mm in size and cleaned by etching in 3% nitric acid solution. The Mg were rinsed with acetone, polished with 800 grit following by 2000 grit SiC polishing paper, sonicated for 30 min in acetone, and finally rinsed with ethanol and distilled water. Both cleaned and polished Mg samples were stored in ethanol until polymer coatings.

The 8-Phe-4 PEA (or Phe-PEA) was provided by the Chu' lab at Cornell university, Ithaca, New York, USA. 8-Phe-4 is a simple homopolymer and was prepared by the solution polycondensation of two monomers: di-p-toluenesulfonicacid salt of bis-phenylalaninebutane-1, 4-diester monomer (Phe-4) and di-p-nitrophenyl sebacate diester monomer (NS). The resulting chemical structure of this 8-Phe-4 is shown in Figure 1. PLGA, MW=100,000, LA:GA ratio =75:25 (Daigang Biology, Shandong, China) was used as a control because it was frequently used in several published degradable polymer coating studies of Mg alloy stents[33-36]. The fundamental properties of 8-Phe-4 and PLGA are listed in Table 1. To fabricate 8-Phe-4 PEA thin coating films, the corresponding 8-

Phe-4 polymer was dissolved in dichloromethane and stirred for 5 h at the concentration of 2%, 4% wt/vol at room temperature. PLGA was dissolved in dichloromethane at the concentration of 2.0% wt/vol.

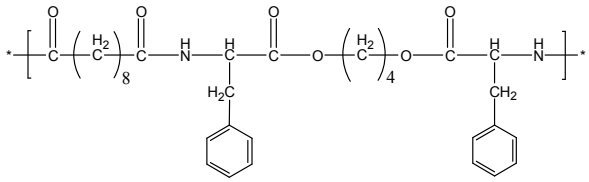

Figure 1. Chemical structure of the repeating unit of 8-Phe-4 poly (ester amide), referred to as 8-Phe-4.

Polymer coating films on Mg substrates were prepared by spin coating as it is the well-accepted method to achieve uniform coating on a simple geometrical Mg model substrate[68]: 100 µL of each polymer solution was dropped onto the surface of Mg sample arranged on the spin coater with a micropipette, the speed of spin coating was set to 200 rpm for 6 sec followed by 6000 rpm for 20 sec, the opposite side of the Mg substrate was prepared likewise. After drying at 37 °C for 48 h in vacuum oven, coatings formed when the solvent evaporated and polymer solidified. Testing samples were labelled as pure Mg (no coating), 2.0% Phe-PEA-Mg, 4.0% Phe-PEA-Mg and 2.0% PLGA-Mg, respectively in this paper, depending on the polymer and its concentration utilized.

2.2. Coating microstructure characterization

Micro-structural observations of the coating surface and its cross section were made for the as-cast and as-coated samples, using a Hitachi s-4800 High resolution SEM at an accelerating voltage of 10 kV. The presence of the coatings was further confirmed by attenuated total reflectance Fourier transform infrared spectroscopy (NICOLET 750, America) using a diamond ATR Smart orbit. Spectra were obtained at 1.0 cm^{-1} resolution averaging 32 scans in the 675–4,000 cm^{-1} frequency range.

The static contact angle of all samples was measured by a Contact Angle Meter (SL200B, Kino, USA) at room temperature (20 °C). The static contact angle was measured by dropping distilled water (2 µL) on the sample surface. Each type polymer-coated Mg was measured in triplicate.

In order to assess the adhesion and elastomeric nature of the Phe-PEA coating on Mg substrates, nano-scratch resistance tests were performed using a nano-scratch option (lateral force measurement) attached in Nano Indenter system (Hysitron, America). The procedure of the scratch is described as following: In the first step, the tip approached the surface under default conditions, and then move 5 µm straightforward along the surface at the set direction to establish baseline; In the second step, the tip loaded at a rate of 33 µN/s to a load of 1000 µN, making the 10 µm distance scratching during the ramp-load scratch procedure; In the third step, we repeat the surface scratching as step 1, and then remove the indenter from the surface of the sample. A diamond Rockwell indenter with a spherical tip was adopted during the scratch process. The nano-scratch resistance tester was also equipped with acoustic sensors to detect the nucleation of the first cracks corresponding to the coating critical load[69]. In addition, the coating surface profile could be sensed and recorded by the depth sensing system, the residual deformation could be photographed. All experiments were performed in a clean environment and 23 °C ambient temperature. At least three similar results were considered valid and their average values were reported for statistical purpose.

2.3. *In vitro* degradation and corrosion

2.3.1. Electrochemical measurement. In electrochemical measurement, the standard method accepted in published literatures was used[35, 70]: a three-electrode cell was used for electrochemical measurements using a CHENHUA CHI650C electrochemical system (Shanghai, China). As-cast and polymer coated Mg samples acted as working electrode, while platinum was used as the counter electrode and saturated calomel electrode (SCE) as the reference electrode. Both electrochemical impedance spectroscopy (EIS) and potentiodynamic polarization curves analysis (Tafel plot) were performed in 125 mL Hank's solution (composed of 8.0 g NaCl, 0.35 g $NaHCO_3$, 0.40 g KCl, 0.06 g KH_2PO_4, 0.01 g $MgCl_2$, 0.14 g $CaCl_2$, 1.00 g glucose, 0.06 g $MgSO_4$, 0.06 g Na_2HPO_4 per litre) at 37.0±0.5°C. The pH of the Hank's solution was adjusted to7.40 prior to the electrochemical test. A working area of 0.196 cm^2 was exposed to the electrolyte.

Electrochemical impedance measurements were performed at open circuit potential (OCP), the amplitude of the sinusoidal perturbing signal was 10 mV, and the frequency varied from 10^5 Hz to 10^{-2} Hz for all the samples. Prior to the EIS measurements, the working electrode was immersed in the electrolytic for 3600 sec until a steady open-circuit potential value was reached. The impedance data was analysed via Nyquist plots.

The potentiodynamic polarization curves (Tafel plot) were measured by polarizing the specimen to -600 mV cathodically and +800 mV anodically relative to the OCP at as can rate of 0.5 $mV{\cdot}s^{-1}$. The corrosion potential and current density was calculated with the Corrview software according to the ASTM-G102-89 standard, based on Tafel extrapolation. The Tafel curves were carried out immediately after the EIS studies on the same exposed electrode surface without any additional surface treatment.

In all the above measurements, at least three similar results were considered valid and their average values were reported.

2.3.2. In vitro corrosion behaviour. Long-term corrosion tests were carried out according to criterion ASTM G31-72, each sample was immersed in 48mL Hank's solution separately in triplicate. Solution temperature was controlled at 37±0.5 °C with a water bath. After prescribed immersion times, the samples were rinsed with distilled water and acetone to remove the corrosion products on the surface. The samples were then quickly washed with distilled water and dried again. The pH value was recorded every 5 days until 30th day as suggested by the criterion in ASTM G31-72 as well as many published magnesium alloy studies[3, 71-73]. Scanning electron microscope (SEM, Hitachi s-4800) equipped with Energy Dispersive Spectrometry (EDS) was used to characterize post-corrosion surface morphology and composition at 10 kV. In addition, the magnesium ion concentration up to 10th and 30th day immersion was assessed by analysing the extracted media after sample incubation. The collected 1mL media was diluted in 4 mL ultra-pure water and analysed using inductively coupled plasma optical emission spectroscopy (ICP-OES, iCAP 6500 Thermo Fisher), 1 mL new Hank's solution replaced the extracted solutions to keep the working condition consistent.

Table 1. Fundamental properties of 8-Phe-4 poly (ester amide) and PLGA samples

Polymer	M_n (kg/mol)	M_w (kg/mol)	M_w/M_n	η_{red} (g/dL)*	T_g (°C)	T_m (°C)	Contact angles θ (°)
8-Phe-4	17.6	23.4	1.33	1.97	40.47	108.111	79.8±0.67
PLGA	57.2	100.0	1.74	1.54	50-55	--	84.50±2.51

*8-Phe-4 data was measured in DMSO at 25 °C concentration=0.25 g/dL[60]

2.4. Cytocompatibility

Rodent vascular smooth muscle cells (VSMC) and human umbilical vein endothelial cells (ECV304) were utilized for cytocompatibility *in vitro*. Cells were cultured in Dulbecco's Modified Eagle Medium (DMEM, HyClone, Beijing) containing 10% fetal bovine serum (FBS, HyClone, Beijing) and 1% penicillin/streptomycin antibiotics (P/S, HyClone, Beijing) at 37 °C, 5% CO_2 and 95% relative humidity.

2.4.1. FE-SEM observation of cells. In cytoskeleton fixing and imaging, the cells were reseeded on the surface of as-cast and as-coated Mg specimens at a concentration of 60,000 mL^{-1}, Tissue culture (plate polystyrene slice) (Costar, USA) acted as a blank control. After the prescribed time (i.e., 12 h), Mg substrates were rinsed with phosphate-buffered saline (PBS, ×1) to remove any non-adherent cells. The remaining cells seeded on the magnesium specimens were fixed in an immobilization solution of 2.5% glutaraldehyde for 120 min at 4 °C. Samples were then rinsed with phosphate-buffered saline (PBS, ×10) before dehydrating through sequential washings in 30, 50, 70, 90, 95, and 100% vol/vol ethanol series in sequence, 5 min each. Finally, samples were immersed in hexamethyldisilazane (HMDS, Aladdin, Shanghai, China) for 15 min instead of critical point dried and kept in dryer before SEM observation at an accelerating voltage of 10 kV.

2.4.2. Cytoskeleton and cellular morphology imaging. Cellular adhesion and morphology were observed using actin and nucleus staining. VSMC cells were seeded on sterilized polymer-coated magnesium substrates at a concentration of 50,000 mL^{-1} and cultured in appropriate media for 24 h and 72 h. Cells were then washed with PBS, fixed using 4% (w/v) paraformaldehyde for 10 min before being permeabilized with 0.1% (v/v) Triton X-100 (Sigma) for 7 min. Following this, cellular actin was stained using 1.0% (v/v) FITC-phalloidin (Sigma) and nuclei were stained using 1 μg/mL DAPI (CST) for 5 min. Cells were imaged using confocal microscopy (A1R-si, Nikon, Japan).

2.4.3. *In vitro* cell viability assay. Rodent vascular smooth muscle cells (VSMC) and human umbilical vein endothelial cells (ECV304) were used to evaluate the cytotoxicity of 8-Phe-4 and PLGA-coated as well as uncoated magnesium samples. Cell viability was tested by indirect (via extract) as well as direct assays according to the protocols of ISO 10993-12:2007.

In the indirect assay, extracts from the polymer coatings were used for assessing their cytotoxicity. Cells were harvested at confluence, counted, and reseeded in 96-well plates at a concentration of 30,000 cells·mL^{-1}, 100 μL per well. Polymer-coated and uncoated Mg samples were placed in 12-well plates and sterilized using UV radiation (254 nm) for 40 min on each side before immersion in DMEM solution with 10% serum for 24 h with a ratio of 1.25 $cm^2 \cdot mL^{-1}$ according to ISO10993-12. At the end of 24 h immersion, the supernatant in the immersed 12-well plates was collected, centrifuged, and then 100 μL of the supernatant/well was added into the 96-well plates with cells. DMEM solution with serum was used as blank control, respectively. 10 μL water soluble tetrazolium-8 (WST-8, Neuronbc, Beijing) was used to test cell viability after cells incubation with extract liquid for 1, 2 and 3 days. Optical density (OD) was tested by microplate reader (Model 680, Bio-Rad, CA) at 450 nm, with the reference wavelength at 630 nm. Cell viability was calculated in accordance with the following formula:

$$\text{Cell viability (\%)} = \frac{OD(test\ sample)}{OD(blank\ control)} \times 100\%$$

In the direct assay, VSMC and ECV304 cells were seeded in 24-well plates (Costar, USA) at a cell density of 1×10^5 cells/well. After seeding 24 h, cells were exposed to the coated and uncoated magnesium samples, DMEM solution with serum was used as a blank control. After incubating for 1, 2, 3 days respectively, the culture media were removed and the specimen were rinsed with PBS buffered three times in order to remove the unattached cells. Cell viability of the adherent cells was measured by adding 500 μL/well culture medium containing 50 μL WST-8 for 4 h incubation. Then 100 μL of supernatant from each well was transferred to new 96-well cell culture plates. Optical density (OD value) of the supernatant was measured and cell viability was calculated in the same way as in the indirect method.

2.4.4. NO release. NO release was tested by indirect (via extract) as well as direct assays. In the indirect assay, VSMC cells were seeded in 96-well culture plates (Costar, USA) at a density of 6000 cells/well, and incubated for 24 h. Then the culture medium was replaced with DMEM with 10% FBS (blank control), extract of bare magnesium, 2% Phe-PEA-Mg, 4% Phe-PEA-Mg and 2% PLGA-Mg. After 24 h incubation, the cell culture supernatant was collected and centrifuged. NO release was tested in new 96-well culture plates by Griess reagent Kit (Beyotime) following the instruction.

In the direct assay, VSMC cells were seeded onto 24-well plates (Costar, USA) at a cell density of 5×10^4 cells/well and were exposed to the coated and uncoated magnesium samples, DMEM solution with serum was used as a blank control. After 24 h incubation, NO release data was tested similarly according to the above method.

2.5. Statistical analysis

All the biological experiments were performed independently at least in triplicate, and three replicates were tested for each experimental point. The data were expressed as means ± standard deviation. The statistical analysis was based on one-way ANOVA analysis of variance, and a p value of less than 0.05 was considered to be statistically significant.

3. Results and Discussion

3.1. Coating characterization

3.1.1. Morphology and coating thickness analysis. The SEM image data (Figure 2) show that as-cast pure Mg substrate (Fig. 2a) exhibited a flat but with only slight remnants of the polishing artifacts and many etched grooves from the final 2000# polishing paper, while the SEM images of 8-Phe-4 and PLGA polymer-coated Mg samples revealed a smooth, dense, non-porous and continuous coating and didn't show any sign of delamination from the alloy substrates (Fig. 2b-d). Besides, 8-Phe-4 coated Mg substrates (Fig. 2c, d) exhibited a smoother surface than the PLGA-coated Mg samples (Fig. 2b). The cross-section morphology data (Figure 3) showed the obvious coating layer when compared with the bare magnesium substrates (Fig. 3a), and the coatings were relatively homogeneous and smooth. The estimated coating thickness was about 4 μm and 12 μm for 2% and 4% 8-Phe-4-Mg, respectively, which was much thinner than the PLGA layer, 16 μm (Table 2). It is interesting to observe that the thicker PLGA coating (Fig. 2b) could not fully cover the groove appearance of a bare Mg substrate, while the 8-Phe-4 coating at both concentrations masked the grooves very

well, even though the thickness of the 8-Phe-4 coatings was only 12.5% of the PLGA thickness at the same polymer concentration.

Table 2. Polymer coating thicknesses on magnesium substrates

Sample type	Estimated thickness(μm)
2.0% 8-Phe-4-Mg	4.0±0.56
4.0% 8-Phe-4-Mg	12.0±1.4
2.0% PLGA-Mg	16.0±1.1

On the whole, 8-Phe-4 coating on magnesium was able to achieve a much smoother and thinner surface than PLGA, which can help to enhance the durability and integrity of the coating. Abdal-hay et al. in their study of the corrosion behavior and cell viability of adhesive polymer coated magnesium based alloys suggested that coating film morphologies (porous or dense structure) can be affected by environmental conditions (ambient or inert atmosphere), solvent type, polymer characterization and its solution concentration and coating method[74]. In the present study, polymer characteristics are the decisive factors that affect coating surface morphologies observed as both 8-Phe-4 and PLGA used the same solvent, concentration and coating method.

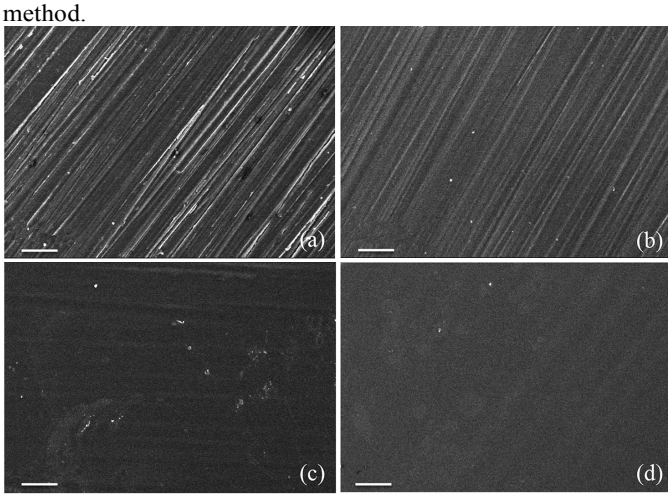

Figure 2. SEM images of the surface morphology of (a) bare magnesium substrates, (b) 2.0% PLGA-coated, (c) & (d) 2%, 4% 8-Phe-4-coated magnesium; Scale bar is 10μm.

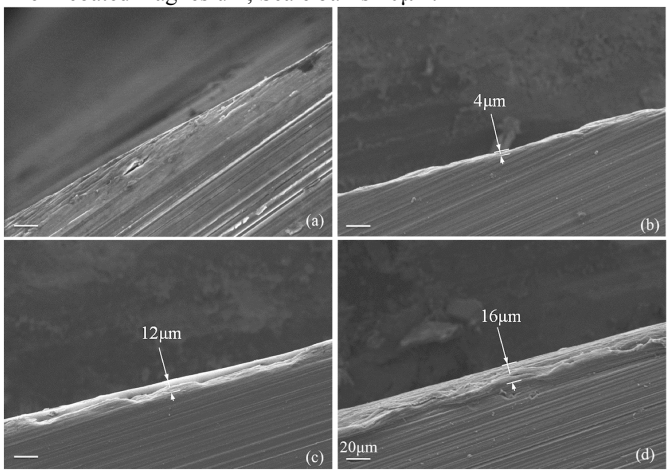

Figure 3. SEM images of the cross-section morphology for coated and uncoated Mg samples. (a) uncoated magnesium substrates, (b) & (c) 2.0%, 4.0% 8-Phe-4-coated and (d) 2.0% PLGA-coated magnesium.

3.1.2. Surface composition analysis. FT-IR was used to verify the presence of the polymer coatings on metal surface. Figure 4 shows the FT-IR spectra of the uncoated Mg alloys (Fig. 4a), 8-Phe-4 (Fig. 4b, c) and PLGA-coated (Fig. 4d) Mg samples. FT-IR spectra show the successful coating of 8-Phe-4 and PLGA onto magnesium substrates. For each testing sample, the coated substrate was compared to spectra of as–cast pure Mg substrate. The characteristic absorption bands in 8-Phe-4, such as carbonyl bands at 1648-1650 cm^{-1} (amide I), 1530-1542 cm^{-1} (amide II), and 1738-1742 cm^{-1} (ester), and broad NH vibration near 3290 cm^{-1} were indicative of the presence of the 8-Phe-4 polymer[58]. The PLGA-coated Mg substrate had the C=O stretching at 1,750 cm^{-1}, C–O–C stretching at 1,080 cm^{-1}, C-H bending peaks at 1500 cm^{-1}, but didn't have the characteristic amide I and II and NH vibration bands observed in the 8-Phe-4-coated Mg samples, which was similar to the previous data[75]. As expect, no such polymer characteristic bands were observed on the bare Mg metal substrates. Moreover, differences between 8-Phe-4 solution concentration and consequently coating thickness have an apparent influence on the relative peak intensity of the obtained spectra, with a positive correlation.

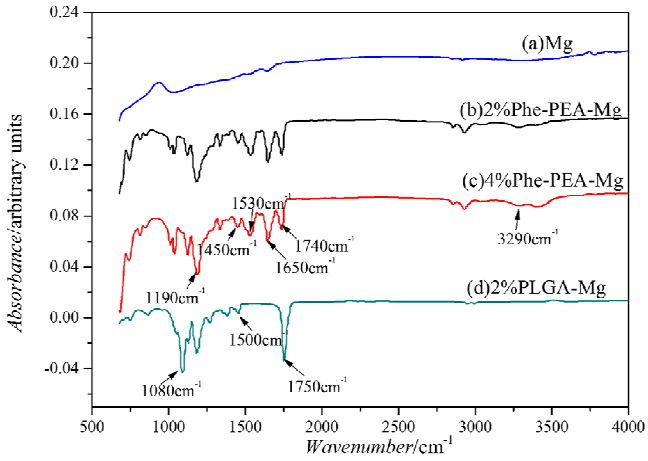

Figure 4. FT-IR spectrum with characteristic absorption bands of (a) bare magnesium, (b) 2% 8-Phe-4 coated, (c) 4% 8-Phe-4 coated and (d) PLGA-coated samples.

3.1.3. Contact Angles. The contact angle data for the coated and uncoated substrates are listed in Table 3. The data showed that the contact angle of the original uncoated Mg samples was 45.4±1.67°, and increased to 63-70° with the 8-Phe-4 coating, and to 75.12° with 2% PLGA coating. Thus, PLGA is the most hydrophobic in the group. An increase in the 8-Phe-4 coating concentration also led to a slight increase in contact angle (63° to 70°), a higher 8-Phe-4 coating concentration led to a thicker coating which provided a more mask and uniform coverage of the underlined Mg substrate and showed contact angles closer to a pure 8-Phe-4 with lesser influence of the underneath Mg substrate, and was consistent with published other

Phe-based PEA films[53]. This result indicated that, via 8-Phe-4 coating, abundant hydrophobic groups, such as phenyl group were introduced to Mg surface which was the key factor that made the 8-Phe-4 coated Mg less hydrophilic.

3.1.4. Nano-scratch resistance. Nano-indentation is a widely used technique for measuring surface mechanical properties at very small scales, Particularly it provides a simple, versatile and rapid means to assess the scratch resistance of the films[69, 76]. The critical point of lateral force in the ramp-load scratch procedure could indicate the coating failure and its correlation with the adhesion strength as well as scratch resistance of the coating. The nano-indentation and scratch data are shown in Figure 5. The critical lateral forces required for initiating coating failure for both 8-Phe-4 coatings at 4% and 2% were significantly higher than the 2% PLGA coated magnesium, i.e., 380 μN at 25 sec - 403 μN at 26 sec for 8-Phe-4 vs. 330 μN at as early as 21 sec for PLGA, a 15-22% higher critical lateral force from 8-Phe-4 than PLGA coating. It is important to consider both the force and time together when analysing the nano-scratch resistance data. These lateral force/time data indicate overall the much stronger adhesion between 8-Phe-4 coatings and Mg substrates than the PLGA coating. The strong adhesion between 8-Phe-4 and Mg substrate can be attributed to strong intermolecular hydrogen bond as evident in the chemical structure of 8-Phe-4 (Figure 1) as well as Van der Waals force between magnesium and 8-Phe-4, but not PLGA. As a result of the strong adhesion between 8-Phe-4 and alloys, both published *in vivo* porcine coronary artery model[39] and human studies[40] of Leu-based PEAs coated 316 Stainless Steel and Co-based alloy stents didn't show any coating delamination.

In all coating groups, there was gross coating spallation detected, and a large area of delamination can be observed from the coating under the critical load condition, similar morphology was also observed in BTSE and octylsilane coated AM60B[69]. The different scratch morphology between 8-Phe-4 and PLGA coatings can be associated with the tensile cracking due to the redistribution of stress induced by plastic deformation of coatings. The clean scratch edge on the PLGA coating suggests the more brittle nature of PLGA than the more elastomeric character of 8-Phe-4. Besides, the depth of the scratch on the 8-Phe-4 coating was much more superficial than the PLGA, indicating the much better elastic resilience of the 8-Phe-4 coating materials, which resulting in the better ability to maintain the integrity as well as durability of the coating. These scratch data are consistent with the lack of cracks and delamination of another Leu-based PEA coating on stainless steel and Co-based stents in both animal and human trial studies[39, 40, 52]. This trait results from the larger elastic modulus of 8-Phe-4 PEA materials.

3.2. *In vitro* degradation and corrosion

3.2.1. Electrochemical measurement. Polarization curves for the uncoated and coated Mg substrates are shown in Figure 6. Table 4 summarizes the corrosion potential (E_{corr}) and corrosion current density (I_{corr}) calculated from extrapolation of the Tafel plots. The 8-Phe-4 coatings on pure Mg substrates resulted in E_{corr} values less negative than the uncoated substrates, implying retard of corrosion happen when compared with a bare magnesium. Moreover, the reduction in I_{corr} values by two orders of magnitude in the 8-Phe-4 coated Mg than the bare Mg sample also corresponded to the least negative E_{corr} values of the 8-Phe-4 coated Mg. In contrast, the PLGA coatings on the Mg substrates resulted in the most negative E_{corr}, and the value is even more negative than the uncoated as-cast Mg, and only a slight diminution in I_{corr} was observed, indicating an inferior barrier function toward corrosion provided by the PLGA. Lu et al.[77], Li et al.[35], and Ostrowski et al.[75] also reported similar reduction of I_{corr} in their PLGA/nickel composite coating on AZ811 Mg alloy, PLGA coating on AZ31, Mg4Y and Mg6Zn alloys.

The I_{corr} values of the 8-Phe-4-coated Mg substrates (0.491-0.602 μA/cm^2) were, however, only a small fraction (4.2-5.1%) of the PLGA-coated Mg samples (11.626 μA/cm^2), and were much lower than the 10% PLGA-coated AZ31 (5.20 μA/cm^2)[75], the phosphate PEO coated WE43 and AZ91D magnesium alloys (about 30 μA/cm^2 and 40 μA/cm^2, respectively)[78], fluoride conversion coated pure magnesium (0.31-8.13 μA/cm^2)[79] and the AZ91 and AM50 magnesium alloys by cerium, zirconium and niobium-based conversion coatings (13-54 μA/cm^2)[80]. As suggested by Cao[81], it is I_{corr} rather than E_{corr} the deciding factor that verdicts corrosion rate, hence we concluded that 8-Phe-4 coating has a far better potential than PLGA in protecting magnesium from over-quick corrosion. The fact that more negative (more active) values of corrosion potential (E_{corr}) correspond to the increase in the rate of corrosion, has also been observed in other published studies by Baril et al.[82] for pure magnesium corrosion in a sulphate medium and by Zhao[83] for corrosion of ZE41 alloy in a chloride medium.

Moreover, there was perceivable difference in the I_{corr} values between 2.0% 8-Phe-4-Mg and 4.0% 8-Phe-4-Mg, of which 4.0% 8-Phe-4-Mg had a thicker coating (about 5 times thicker than 2.0% 8-Phe-4-Mg). This thicker 8-Phe-4 coating appeared to have a more beneficial effect toward the reduction in I_{corr} value (an 18% reduction from the I_{corr} of the 2.0% 8-Phe-4-Mg), indicating the potential advantage of 8-Phe-4 or other AA-PEA biomaterials as magnesium coating.

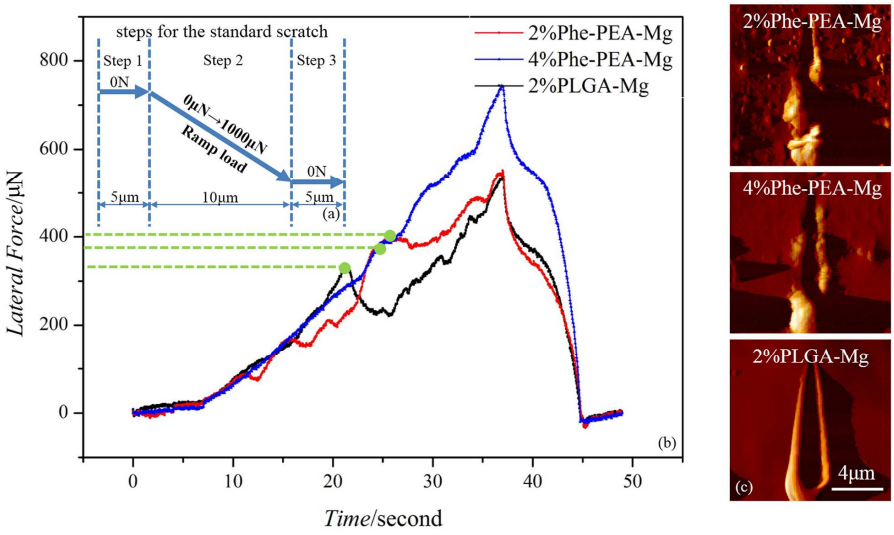

Figure 5. (a) Steps for the standard nano-scratch resistance test; (b) lateral forces changed with time during the nano-scratch resistance tests were recorded for 2%, 4% 8-Phe-4 coated and PLGA-coated Mg samples, green dots signifies the critical point of the lateral forces fluctuations; (c) residual deformation morphology of the samples.

Table 3.Water contact angle (θ) for bare magnesium, 8-Phe-4 coated and PLGA-coated Mg samples

	Mg	2% Phe-PEA-Mg	4% Phe-PEA-Mg	2.0% PLGA-Mg
Contact Angle θ/°	45.4±1.67	63.01±2.90	70.12±1.55	75.12±1.29

The observed difference in electrochemical data among the testing samples is a consequence of the difference in the polymer chemical structure between 8-Phe-4 and PLGA coating biomaterials. The chemical structure of 8-Phe-4 differs from PLGA mainly due to the presence of an amino acid that provides amide linkages in addition to ester linkage, while PLGA has only ester linkage. This amino acid moiety in 8-Phe-4 could lead to stronger hydrogen bonds between macromolecular chains and Mg substrate, thus a stronger binding force and a more stable polymer layer could be formed, resulting in a stronger anti-corrosion ability, even though 8-Phe-4 had a thinner coating than PLGA.

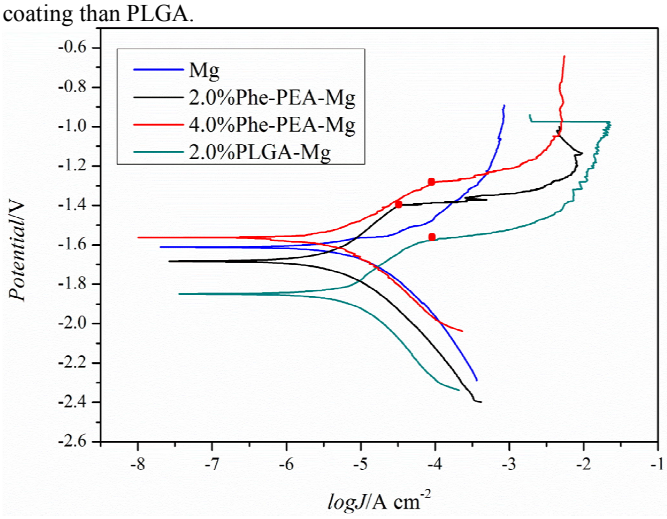

Figure 6. Tafel plots for bare magnesium, 8-Phe-4 coated and PLGA-coated Mg samples; the red dots signifies the breakdown potential (E_{bd}) at 2000 s and 2200 s for 2% and 4% 8-Phe-4 coating, respectively.

It should be noted additionally that a breakdown potential (E_{bd}) referred to the potential of the substrate at which coating is broken down appeared in the anodic branch of the polarization curve for the coated samples (marked by the red dots in Fig. 6), suggesting the destruction of the protective films at about -1.60 V, -1.40 V and -1.25 V for 2% PLGA, 2% and 4% 8-Phe-4 coating, respectively during the experiment. While more negative E_{bd} than 8-Phe-4 coated magnesium was observed on the cerium, zirconium and niobium-based conversion coatings on AZ91 and AM50 (-1.90 ~ -1.70 V)[80] and phosphate PEO coated WE43 and AZ91D magnesium alloys (-1.50 ~ -1.65 V)[78].The less negative the breakdown potential value of the surface layer indicates a much more compact and stronger-bond coating of 8-Phe-4 onto the magnesium.

The breakdown of initial pitting corrosion of Mg alloy ZE41 was similarly observed in Tafel plots by Zhao et al.[83] in their study of influence of pH and chloride ion concentration on the corrosion of Mg. Wang et al.[84] attributed such a breakdown to the Cl^- ions which made the oxide film of Mg-Al-Pb and Mg-Al-Pb-Zn-Mn alloys breaking down during the potentiodynamic polarization test.

The Nyquist plots for the corrosion of the bare Mg, 8-Phe-4-coated as well as PLGA-coated Mg in Hank's solution at 37 °C are shown in Figure 7. The Nyquist plots presented two capacitive loops at higher and medium frequency, followed by an inductive loop at a lower frequency region. The higher frequency semicircle was ascribed to oxide film effects and charge transfer in corrosion process, and the medium frequency semicircle signified mass transfer such as diffusion of magnesium ions in solid phase through the corrosion product layer. The lower frequency inductive loop was assigned to the relaxation of surface adsorbed species like $Mg(OH)_2$. Similar observation was also obtained from AZ91 alloy in 1M NaCl solution[85] and from cross-linked gelatin/PLGA nanoparticles coating on the MAO film of magnesium alloy stent materials WE42 in Hank's solution[33]. Further, the Z_{re} values (Z' value when Z'' value is 0, an important impedance indicator in EIS studies, the higher Z_{re} indicates the higher anti-corrosion ability) of both 8-Phe-4 (14,800 ohm·cm^2) and PLGA-coated (15,000 ohm·cm^2) Mg samples are much higher than the bare sample (11,800 ohm·cm^2), indicating the similar electrochemical impedance spectroscopy of 8-Phe-4 when compared to PLGA, thus providing an equal capability in inhibiting

magnesium corrosion. This value of 8-Phe-4 coated magnesium alloy was larger than what has been reported for protective diffusion coating of Nd for Mg-1.2%Nd-0.5%Y-0.5%Zr-0.4%Ca magnesium alloy (about 11,000 ohm·cm^2 after 24 h immersion) and the value of hydrofluoric acid treated AZ31 magnesium alloy (about 3,000 ohm·cm^2) for different hours in 3.5% NaCl solution[86]. Roughly, the 4% 8-Phe-4 coated Mg samples (red triangle in Fig. 7) showed slightly larger capacitive loops than the 2% PLGA-Mg coated ones (green dots in Fig. 7), while the 2% 8-Phe-4 coated ones (black square in Fig. 7) exhibited slightly smaller capacitive loops. As the enlargement of capacitive loops has a positive correlation with reduced corrosion rate, the passable performance of 8-Phe-4 in corrosion resistance could be concluded. The above explanation of EIS curve has been the most popular interpretation[82, 87], although interpretation for EIS data of magnesium alloys has never reached a consensus, with a few other versions proposed[88].

Therefore, the less negative E_{corr} value and significantly lower I_{corr} values in the Tafel plots in the 8-Phe-4 coated Mg substrates (Table 4) combined with their larger capacitive loops in the Nyquist plots (Fig. 7) indicate that the 8-Phe-4 coating had better anti-corrosion capability for magnesium when compared with the PLGA coating.

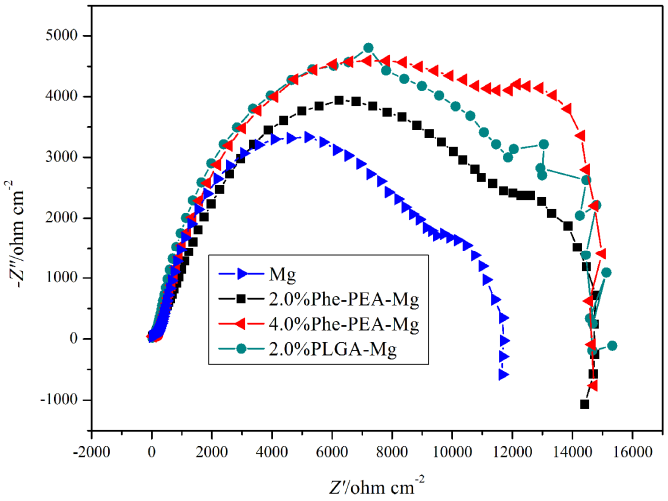

Figure 7. Nyquist plots for bare magnesium, 8-Phe-4 coated and PLGA-coated samples; the enlargement of capacitive loops has a positive correlation with reduced corrosion rate.

Table 4. Corrosion potential (E_{corr}) and current density (I_{corr}) values for coated and uncoated Mg substrates

Sample type	E_{corr} (V)	I_{corr} (μA/cm^2)
Pure Mg	-1.612	16.011
2.0% 8-Phe-4-Mg	-1.583	0.602
4.0% 8-Phe-4-Mg	-1.564	0.491
2.0% PLGA-Mg	-1.770	11.626

.

3.2.2. *In vitro* corrosion behaviour. According to current recommendations in ASTM G31-72[89, 90], both the coated and uncoated Mg substrates were further immersed in the Hank's solution at 37 °C for 30 days to qualitatively determine the polymeric coatings effect on the corrosion resistance ability and the degradation rate of the magnesium.

SEM images as well as corresponding EDS spectrogram of the substrates after 10 days (Fig. 8a-d) and 30 days (Fig. 8e-h) immersion in the Hank's solution at 37 °C are shown in Figure 8. The PLGA-coated Mg samples showed large cracks and serious delamination at both the 10th and 30th day immersion. Similar cracks were also observed on poly (l-lactic acid) and poly (ε-caprolactone) coated magnesium[91] under cell culture condition, even some gas bubbles resulted from trapped hydrogen gas underneath the polymeric surface during 3 days incubation formed on PLGA coated AZ31 and Mg4Y[75]. While the 8-Phe-4-coated Mg samples showed few such bubbles because the gas evaporated from the narrow cracks before it was able to gather and lead to the collapse of the gas bubbles.

In addition, as it was shown in the EDS data, the PLGA-coated Mg substrates had much more crystal and precipitation products consisting of Ca, P and O elements over the last 20 days immersion than the first 10 days, which could also be observed from the corresponding SEM images with a lot of cylindrical or spherical crystals. Moreover, from the cursory EDS quantification of the 30th day, it was calculated that the Ca/P ratio on the PLGA-coated Mg substrate was 1.77, which was similar to the 1.67 ratio in hydroxyapatite [$Ca_{10}(PO4)_6(OH)_2$], suggesting hydroxyapatite (HA) crystals were likely to have formed on the PLGA-coated substrates. Similar EDS pattern of dicalcium phosphate dihydrate brushite crystals formed on AZ31 magnesium alloy, which is a precursor to the more stable phase hydroxyapatite[92]. The formation of large cracks and delamination as well as deposited HA on the PLGA-coated Mg substrate would be harmful for blood when used as stents because Witte et al. reported that hydroxyapatite particles could cause the aggregation of erythrocytes[93], which could lead to a higher blood viscosity, and the potential to promote blood clotting[38].

For the 8-Phe-4 coated Mg substrates, however, the cracks were much fewer and more superficial, no obvious delamination was observed, thus suggesting a better anti-corrosion ability than PLGA. Contrary to the PLGA-coated Mg sample, no HA formed on the 8-Phe-4 surface as the Ca/P ratio was only 1.19, and much smaller Ca and P peak intensity (i.e., indicating less level of calcium phosphate deposited on the 8-Phe-4 coated Mg sample surface). This different degradation morphology between 8-Phe-4 and PLGA was attributed to their difference in surface chemistry and degradation mechanism as 8-Phe-4 degrades via a surface degradation mechanism, while PLGA degrades via a bulk mode.

The pH values of the Hank solution was measured every 5 days up to 30th day as pH data can also reflect the corrosion behavior of magnesium samples. Figure 9 shows such pH data of the testing and control Mg samples. The in vitro corrosion of magnesium followed the general reaction, thus causing an alkaline atmosphere which led to a higher pH value.

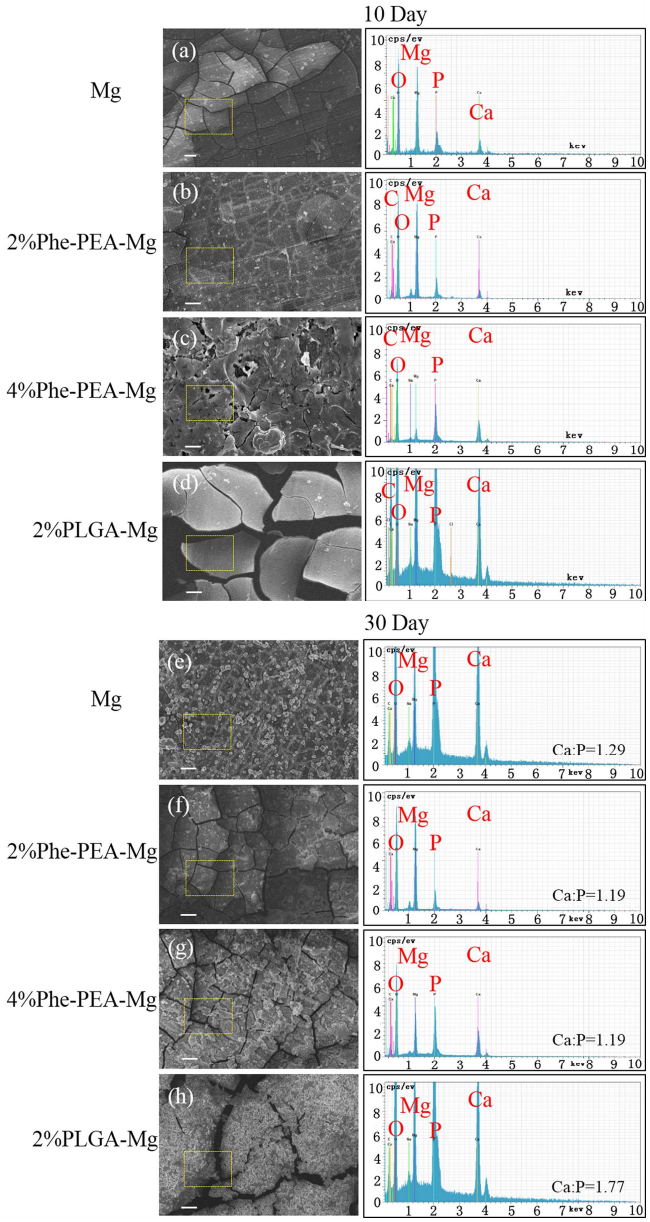

Figure 8. SEM images of the bare magnesium, 8-Phe-4 and PLGA-coated Mg samples after 10 (a-d) and 30 days (e-h) immersion in the Hank's solution; The EDS spectra show both Ca, P, and Mg peaks. Scale bar is 10μm.

All testing Mg samples showed an initial pH increase from 7.4 to above 8 over the first 5 days of immersion. The uncoated Mg substrate reached a high pH of 9.2 at the end of 30 days testing period. However, both the 8-Phe-4 and PLGA coating were able to deter the solution from becoming excessively alkaline as the pure Mg substrate did which overpasses local tissue receptivity. The 8-Phe-4 coated Mg substrates, however, exhibited lower pH values than the PLGA-coated ones over the whole testing period with a noticeable but slight initial decline at 10th day, following by a slight increase thereafter, and reached a steady pH between 8.2-8.3. The PLGA-coated Mg substrates showed a continue increase in pH beyond 10 days irrespective of the fact that the degradation products of PLGA are well-known for their acidic nature. The pH data (Fig. 9) show that 8-Phe-4 reached a pH only 8.2-8.3 at the end of 30 days immersion which is far lower than all those reported treated or coated Mg alloys. For examples, the pH of AZ91D magnesium alloy treated with physiological stabilization-hydrothermal process was higher than 10.0 after 15 days immersion in Hank's at 37 °C[94], Mg80-OLA20 reached pH as high as 9.5 under harsh conditions (80 °C and 100 rpm) over 21 days[95], alkali-heat-treated Mg reached as high as 10.1 at 14th day in SBF solution[96], fluoride treated AZ31B reached 10.2 at 30th day in the simulated body fluid[14], MAO-treated Mg-Ca alloy samples reached 8.7-10.5 at the 30th day immersion in Hank's solution[70], PLA-coated high purity magnesium topped 7.9 at the end of 8th day immersion in m-SBF and showed a continuous sharp growing trend[97].

As for the PLGA-coated Mg samples, the pH value increased steadily over the whole period and reached a pH of 8.9 at the end of 30 days, a pattern very similar to the pure magnesium control. The bulk degradation mode of PLGA could lead to the penetration of water molecules through PLGA layer into the underneath Mg substrate, and the formation of large cracks could aggravated this effect: faster corrosion of the underneath magnesium substrates.

Therefore, the 8-Phe-4 coating provided a steadier local *in vitro* pH environment far more acceptable than the PLGA coating. As a whole, 8-Phe-4-coated Mg samples showed more significant barrier function in effectively controlling pH value within physiological limits, even though 8-Phe-4 had a thinner coating than PLGA. For both of these two polymer species, coating of various thickness may provide initial protection of the magnesium surface, but the integrity and stability of the coating materials would need further improvement for providing better performance of the Mg-based stents.

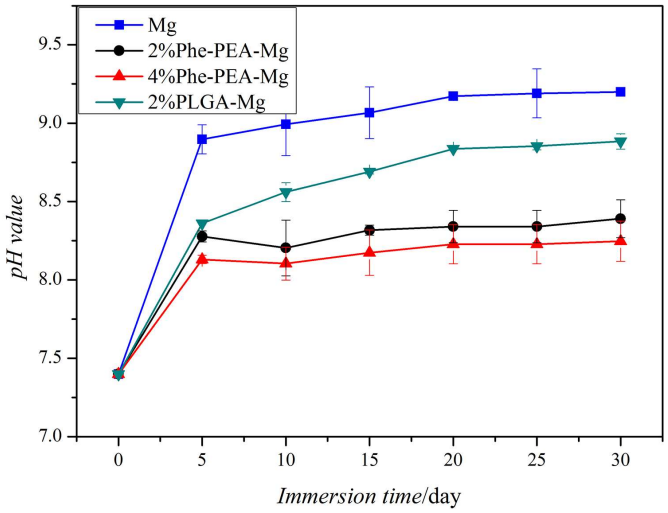

Figure 9. pH values of the Hank's solution with bare magnesium, 8-Phe-4 coated and PLGA-coated Mg samples up to 30 days immersion at 37 °C; the initial pH value of the Hank's solution is 7.4.

The ICP-OES protocol was adopted to measure released magnesium ion concentration from bare Mg, and polymer-coated Mg samples after immersion in the Hank's solution for 10 and 30 days. It is useful to identify the localized Mg ion concentration in the near vicinity of the Mg stent implant, as such local Mg ion concentration is an important factor in considering the biocompatibility of the Mg biomaterial. Figure 10 shows the Mg dissolution profiles based on the soluble magnesium ion released over a 30 days period under an in vitro culture conditions. Both 8-Phe-4 and PLGA coatings

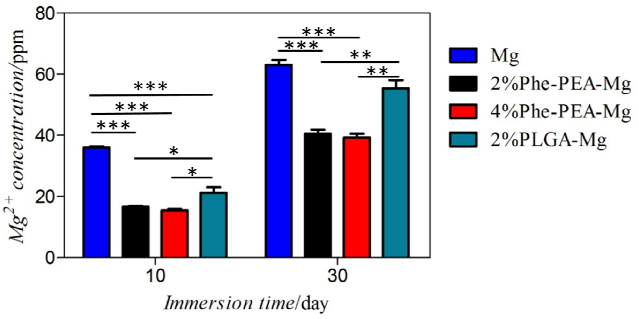

Figure 10. Magnesium ion concentration released from bare magnesium, 8-Phe-4 coated and PLGA-coated Mg samples after 10 and 30 days immersion in Hank's solution; * represents $p<0.05$, ** represents $p<0.01$, *** represents $p<0.001$.

significantly reduced the magnesium ion released when compared to a bare Mg control, indicating an effective barrier function from the polymer coatings. Most importantly, the 8-Phe-4 coated Mg samples (about 18 ppm at 10th day, 40 ppm at 30th day) released far less Mg^{2+} than the PLGA-coated samples (about 21 ppm at 10th day, 57 ppm at 30th day) over the whole period, i.e., 14-30% reduction in Mg ion concentration in the Phe-PEA coated Mg sample. Besides, these released Mg ion value from the 8-Phe-4 coated Mg alloy was much lower than the physiological stabilization-hydrothermal treated AZ91D magnesium alloy after 15-day immersion (about 80 $\mu m \cdot mL^{-1}cm^{-2}$)[94], the polymeric layer-by-layer (PEI-PCL-PAH) coated AZ31 (accumulated Mg^{2+} value is about 13 mmol in 7-day extracted incubation media)[98] and the 10-day PLLA or PCL coated Mg (accumulated Mg^{2+} value was about 80-100 ppm)[91]. These Mg ion concentration data are consistent with the observed degradation morphology and pH value data given above. The amounts of the released Mg^{2+} became lower as the concentration of the 8-Phe-4 coating became higher, which is also in correspondence with the data from the electrochemical tests, SEM images and pH value above.

3.3. Cytocompatibility

3.3.1. Cell morphology. Cellular behaviour and response is a vital factor in the evaluation of biomaterial biocompatibility[99]. Generally speaking, the cells will undergo their morphological changes to stabilize the cell-material interface after contacting biomaterials. During the process of adhesion and spreading, cell attachment, filopodial growth, cytoplasmic webbing, flattening of the cell mass and the ruffling of peripheral cytoplasm proceed in order[100]. The SEM images of adhesion and attachment of rodent vascular smooth muscle cells (VSMC) 12 h (×2000, ×100) and 24 h (×100) after seeding on the bare and coated Mg samples are shown in Figure 11. At the 12 h incubation period, only 13±3 VSMC cells/mm^2 was observed on the bare magnesium surface other than cracks and coralloid depositions (Fig. 11b). In contrast, significantly higher numbers of VSMC attached onto the 4% 8-Phe-4 (86±7 cells/mm^2, Fig. 11h) and 2% 8-Phe-4 (71±6 cells/mm^2, Fig. 11e) coated magnesium respectively, which approximated the VSMC cell number (115±12 cells/mm^2) adhered on the tissue culture plate (Fig. 11n). These VSMC cells on the Phe-PEA surface were statistically advantageous over the PLGA-coated magnesium surface (56±5) (Fig. 11k), and were much more than the osteoblasts proliferation (2100 cells/cm^2) after 1 day of culture on bredigite ceramics[101], indicating a favourable adhesion of VSMC on 8-Phe-4 coated magnesium. The 24h VSMC cell data showed almost the same level as the 12h data.

In addition to the advantage in the number of attached VSMC cells over a bare Mg metal, the VSMC cells on the surface of the 8-Phe-4 coated (Fig. 11d–i) and PLGA-coated surface (Fig. 11j–l) showed flattened, extended and spread cell morphology, and the cells on the surface of the 8-Phe-4 coatings were more flattened and showed longer pseudopod than the ones on the PLGA-coated substrates. Therefore, 8-Phe-4 coating had a better cytocompatibility as well as more obvious effect in reducing harmful Mg corrosion products than PLGA coating.

The data in Fig. 11 also showed that the formation of coating exfoliation and corrosion products on the surface played a direct role in the location and the manner in which the cells grew. i.e., severe exfoliation coating pattern and large corrosion products (indicated by the white arrows in Fig. 11k) appeared on 2.0% PLGA-Mg (Fig. 11k) led to a lower level of cell attachment as high density of cells were localized in the flat region without obvious corrosion products, but no cells were found in the corrosion product regions or bare substrates, especially in the 24 h data. This is likely due to the increased alkalinity in those local regions due to soluble by-products formed such as magnesium ion. The coating layer of 8-Phe-4 remained smooth and intact, on which larger number of cells distributed more uniformly.

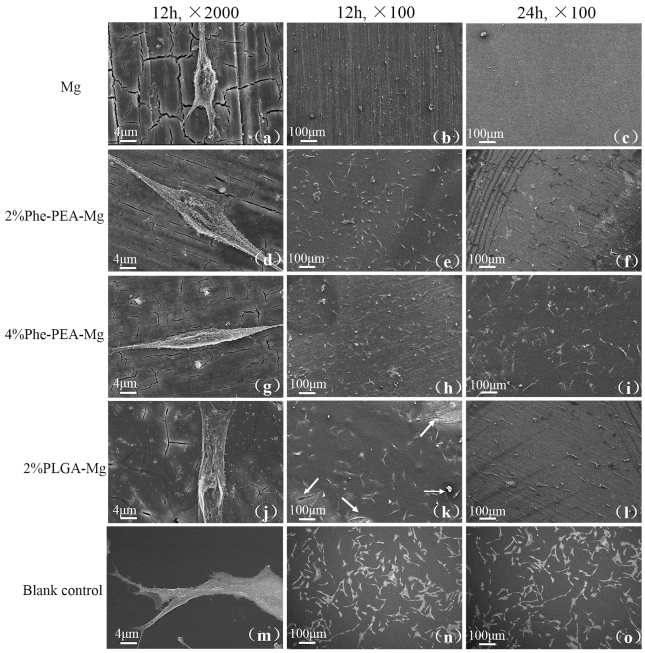

Figure 11. SEM images of adhesion and attachment of rodent vascular smooth muscle cells (VSMC) 12 h and 24 h after seeding on the bare magnesium, 8-Phe-4 and PLGA-coated magnesium samples. Tissue culture plate (polystyrene slice) acted as blank control.

Actin staining of VSMC 24 h and 72 h post seeding can be seen in Figure 12, the long green bundles of stress fibers composed of actin filaments and good cell-cell contact with one another demonstrated the good cell cytoskeleton morphology of the VSMC cell adhered on the substrates. Notably, markedly more cells adhered on the surface of 8-Phe-4 coated magnesium than the bare magnesium and PLGA-coated group, indicating that the VSMC was more favourable of adhering onto the more biocompatible 8-Phe-4 coated substrates. VSMC cellular morphology was triquetrous and poorly defined on the uncoated magnesium (Fig. 12a-d), without strong actin fiber staining, indicating that the cells are likely poorly adhered to the substrate. Cells on the 2% PLGA-coated magnesium (Fig. 12m-p) became elongated while cells on the 2% 8-Phe-4 (Fig. 12e-h) and

4% 8-Phe-4 (Fig. 12i-l) coated substrates appeared well spread out, with strong actin filaments extending in numerous directions and exhibited a rearranged cytoskeleton with better-developed stress actin fibers and stronger actin intensity[102], suggesting that the 8-Phe-4 coated magnesium possessed much better cell adhesion and spreading. It has been postulated that the reduced cell densities and abnormal cellular morphology on the PLGA coated magnesium is due to the inherent PLGA bulk degradation, allowing water to contact the magnesium surface, and acidic polymer degradation products increasing the solubility of the passivation layer that would otherwise form on areas of the metal exposed to water. Additionally, the resulted bubbling effect may create localized galvanic corrosion effects.

Generally, cell adhesion, spreading, proliferation and migration on substrates are the first sequential reactions while cells come into contact with a material surface; therefore, materials cytocompatibility is the top priority for cell survivals. The observed extensive spreading and attachment of the vascular smooth muscle cells (VSMC) onto the 8-Phe-4 coating illustrates that this new 8-Phe-4 coatings should have a better biological property than PLGA coatings as demonstrated later in the cell viability data (Figures 13&14).

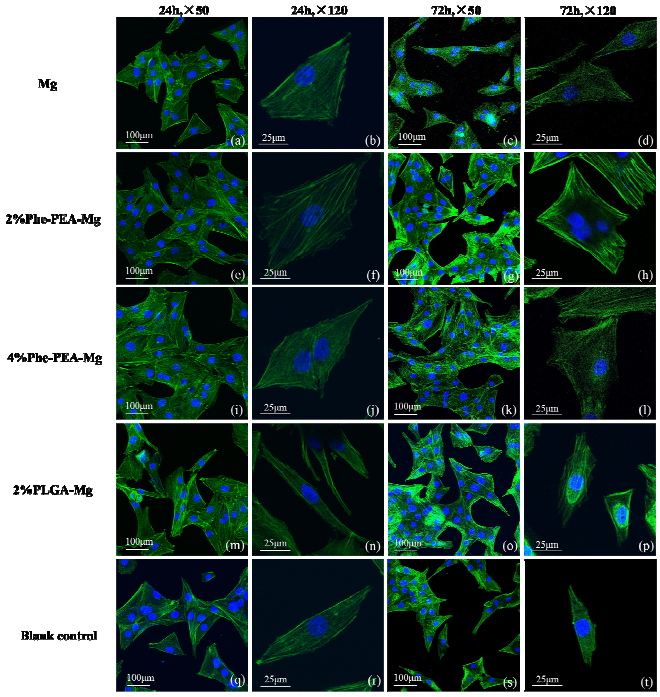

Figure 12. Rodent vascular smooth muscle cell (VSMC) morphology observed at 24 h and 72 h post seeding through actin-nucleus co-staining on (a-d) bare Mg, (e-h) 2% 8-Phe-4, (i-l) 4%8-Phe-4, (m-p) 2% PLGA coated magnesium, and (q-t), blank control tissue culture plate.

3.3.2. *In vitro* cell viability assay. Figure 13 shows the cell viability of both rodent vascular smooth muscle cells VSMC (Fig. 13a) and human umbilical vein endothelial cells ECV304 (Fig. 13b) grown in the extracts of the polymer-coated Mg substrates for 1, 2, 3 days as determined by the CCK-8 assay. All the extracts of the polymer-coated 8-Phe-4 and PLGA samples significantly improved viability of the VSMC and ECV304 with the cell growth rate ranging from 113.0%-76.3% and 91.5%-79.2% respectively over the whole period, compared with the uncoated Mg samples (ranged from 71.9% to 79.0%).Thus, the extracts from both 8-Phe-4 and PLGA-coated Mg substrates could significantly ($P<0.05$) improve cell viability relative to the bare magnesium. In the PLGA group, 2 days viability reached to a peak in VSMC case, while the 2% and 4% 8-Phe-4 coated Mg samples showed continuously increase in cell viability with incubation time in both VSMC and ECV304 cases, which are ascribed to the better cytocompatibility of the 8-Phe-4. For ECV304 cells, the 8-Phe-4 group showed a continuous advantage over PLGA group as time went on, confirming the potential of more notable effect in accelerating endothelium healing. When comparing with the blank control (tissue culture plates), the 8-Phe-4 coated Mg substrates show the same or higher cell viability in both cell types, particularly the VSMC (Fig. 13a). When comparing with other published studies, the cell viability data of the 8-Phe-4 group for both VSMC and ECV304 were much higher (>100%), such as the L-929 cell viability (28%-70%) cultured in phytic acid modified WE43 Mg extraction solution for 1, 2 and 4 days[5], the HEK293 cells viability (78%-91%) for physiological stabilization hydrothermal treated AZ91D magnesium alloy for 1, 3, 7, 15 days[94], the HEK293 cell viability incubated with BMS-Br (68%) and BMS-g-HPBBEA (76%)[103], the MG63 cell viability (about 82%-93%) cultured in MAO-treated Mg-Ca alloy sample extracts for 1, 3 and 5 days[70], the HUVECs proliferation profile (30%-70%) cultured with calcium silicate extracts diluted with control medium at 1/4 dilution ratios at 3, 7 days[104].

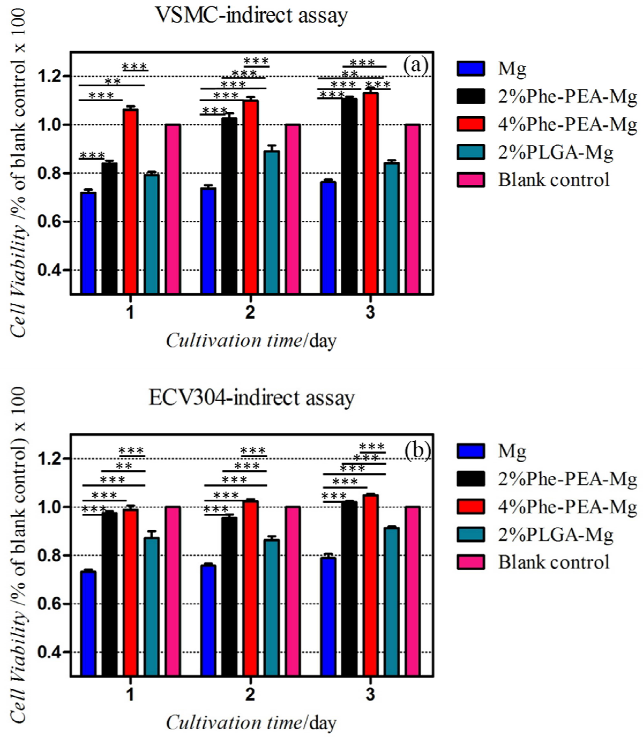

Figure 13. Cell viability cultured in the extracts of the bare magnesium, 8-Phe-4 and PLGA-coated samples by the CCK-8 assay over 3 days incubation period: (a) VSMC and (b) ECV304; DMEM with serum acted as blank control; *** represents $p<0.001$, ** represents $p<0.01$.

Figure 14 shows the cell viability after seeding the cells directly onto both 8-Phe-4 and PLGA-coated Mg substrates instead of their extracts so that the cellular behaviour on direct contact with the coating biomaterials could be elucidated. The cell viability data show that the 8-Phe-4 coated Mg samples had significant advantages over both PLGA-coated and bare Mg samples. i.e., 15.0-58.8% higher than PLGA and 21.5-70.1% higher than bare Mg samples for both VSMC and ECV304. On the contrary, the PLGA-coated and

bare Mg showed similar viability with PLGA group edging slightly better over the whole period. Moreover, the 8-Phe-4 coating advantage showed up as early as 1st day culture and lasted till 3rd day, of which its early advantage at 1st day indicated the potential of 8-Phe-4 to promote cell proliferation faster than the blank control. In accordance with the direct assay data, the 2% 8-Phe-4 coated Mg samples had an advantage over 4% 8-Phe-4 initially, but this benefit became less with the time, indicating the long-term ability of 8-Phe-4 to inhibit Mg corrosion. Although 8-Phe-4 coated Mg showed graduate reduction in cell viability with time, but their viability for both VSMC and ECV304 were still significantly higher than PLGA-coated and bare Mg. The graduate reduction in cell viability after 1st day culture in 8-Phe-4 is probably due to the correction of initial over population beyond monolayer. Compared to the indirect extract assay, cells were in direct contact with magnesium samples in the direct assay, hence, the characteristics of the coating material could be reflected more significantly. Moreover, the testing samples in the direct assay were immersed for much longer time, thus the degradation phenomena of both polymers and magnesium in the culture medium could affect the outcome of the cell viability data. Combining these two features of the direct assay mentioned above, we could conclude a more obvious advantage of 8-Phe-4 over PLGA in biocompatibility when used as magnesium coating.

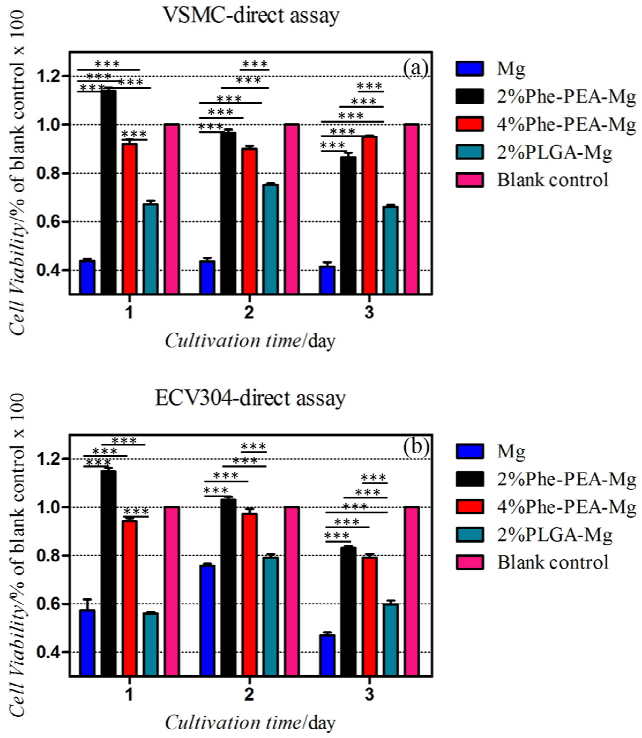

Figure 14. Cell viability cultured on bare magnesium, 8-Phe-4 and PLGA-coated magnesium samples by the CCK-8 assay over 3 days incubation period: (a) VSMC and (b) ECV304; DMEM with serum acted as blank control; *** represents $p<0.001$.

3.3.3. NO release. NO release data of vascular smooth muscle cells (VSMC) incubated via both indirect and direct assays of each group of substrates are shown in Figure 15. In the indirect assay, NO release for the 8-Phe-4 coated Mg samples extracts were about 3.1 $\mu m \cdot L^{-1}$ and 3.5 $\mu m \cdot L^{-1}$, respectively, and was significantly higher than the PLGA-coated samples (1.9 $\mu m \cdot L^{-1}$) and bare Mg samples (1.7 $\mu m \cdot L^{-1}$), the 8-Phe-4 data were even higher than the blank control group (2.5 $\mu m \cdot L^{-1}$). Previous studies proved the ability of NO to inhibit vascular smooth muscle cell proliferation[105-107] besides the role of vascular tension regulation as a local produced vascular active substance. Hence, we may conclude that the higher NO release of 8-Phe-4 coated magnesium lead to its better ability in prohibiting VSMC growth, thus minimizing the risk of restenosis caused by hyperplasia endothelialis. In the direct assay, the NO data of the 8-Phe-4 groups were higher than the corresponding one from the indirect assay (e.g., from 3.1-3.6 $\mu m \cdot L^{-1}$ at indirect assay to 3.3-4.3 $\mu m \cdot L^{-1}$ at direct assay). The NO release in the PLGA and bare magnesium groups, however, decreased in the direct from the indirect assay. Therefore, coupled this NO data with the cell viability data given in Figs. 13 and 14, the 8-Phe-4 coating on Mg substrates not only provided far better cell viability but also more biological functionality like NO secretion than the PLGA coating.

Compiling the results of cell adhesion, cell viability and NO release given above, it is clear that the biocompatibility of the 8-Phe-4 coating excels PLGA, which is reflected in the ability of 8-Phe-4 coating to significantly improve VSMC as well as ECV304 viability over PLGA. The difference in the chemical composition between 8-Phe-4 and PLGA should bear the cause behind this drastic difference in both types of cellular responses. In their study of bovine endothelial cell adhesion on a variety of cationic, anionic and neutral functional AA-PEAs, Horwitz et al.[60] reported the cells are able to spread, assemble a cytoskeletal network, and form specific integrin mediated adhesion with the AA-PEA substrate. They concluded that the AA-PEA tested could remodel the AA-PEA substrate surface with cell-adhesion proteins like vinculin resulting in the formation of specific integrin-mediated adhesion of the cell to the substrate. Our VSMC and ECV304 cell viability data on 8-Phe-4 coated Mg substrates are consistent with the Horwitz et al. study.

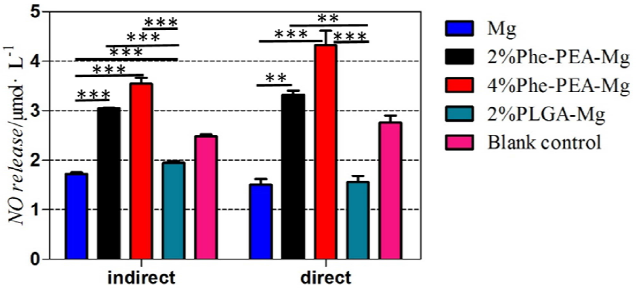

Figure 15. NO release from VSMC cell cultured in the extract of bare magnesium, 8-Phe-4 and PLGA-coated magnesium samples (indirect assay) and onto bare magnesium, 8-Phe-4 and PLGA-coated magnesium samples (direct assay) over 24 h incubation period; DMEM with serum acted as blank control; *** represents $p<0.01$.

In addition to the chemical composition factor, the different modes of degradation mechanism between 8-Phe-4 and PLGA may also play a role in the different corrosion-resistance level. The relatively inadequate corrosion-resistant nature of PLGA coatings on the surface of magnesium may result from their bulk degradation mechanism, where the material loses volume throughout as opposed to surface degradation mode from 8-Phe-4 coating, where degradation is mainly confined to the outmost surface layer like peeling an onion[37]. The bulk degradation of the polymeric coating such as PLGA leads to the total exposure of the coating to water molecules and the acid nature of the PLGA degradation products (glycolic and lactic acids) that could accelerate magnesium corrosion. In the case of 8-Phe-4 coating, it undergoes a surface degradation, mostly according to zero-order kinetics, and their biodegradation rate in *in vitro* such as a pure saline buffer or simulated body fluid is

slow (several months to years)[58, 66]. Jokhadze et al. reported that the degradation products of a generic AA-PEA homopolymer are aliphatic diols (one of the 3 building blocks of AA-PEAs) and N, N-dicarboxylic (bis-amino acid). The corrosion data in our current study suggest that the surface degradation mode along with the type of degradation products from 8-Phe-4 coating appear to result in a more desirable corrosion-resistant performance and better cytocompatibility than the popular PLGA coating on Mg metal substrates.

Conclusion

A new biodegradable phenylalanine-based poly (ester amide)s (8-Phe-4) biomaterial was spun-coated onto a magnesium substrate as a model for the purpose of providing a better protective shield to counter the common corrosion problem associated with Mg-based biomaterials. The commonly used hydrolytically degradable PLGA was chosen as the control for assessing the performance difference between the new 8-Phe-4 coating and the traditional PLGA coating on Mg substrates. Both 8-Phe-4 and PLGA could form a smooth, dense, non-porous and continuous coating layer on Mg substrates with strong bonding, even though the 8-Phe-4 had a much thinner and better scratch resistant coating which masked the groove feature on Mg substrates better than PLGA at the same concentration. The better plastic deformation property of 8-Phe-4 than PLGA was achieved at a lower MW of 8-Phe-4 than PLGA. Standard electrochemical measurements (corrosion potential and current density) demonstrated that the 8-Phe-4 coating had a significant advantage over the PLGA coating in anti-corrosion behaviour. Moreover, the level of retention of surface morphology integrity, pH value change as well as the amounts of magnesium ion released in a controlled *in vitro* environment also indicated that the 8-Phe-4 coating showed better improvement of magnesium corrosion resistance performance over the PLGA coating. In addition, rodent vascular smooth muscle cell and human umbilical vein endothelial cells showed far better cell viability and cell function adhered onto the 8-Phe-4 coated Mg substrates than both PLGA-coated and uncoated Mg. Therefore, the current *in vitro* data suggest that the newly developed biodegradable amino acid-based poly (ester amide) biomaterials (AA-PEA) may have the potential as the coating for the Mg-based biomaterials for enhanced their anti-corrosion and cytocompatibility.

These encouraging *in vitro* data obtained in the current study will provide us with a better foundation to use a real Mg stent model with a complex geometry to validate our *in vitro* data in a subsequent future *in vivo* animal trial.

Acknowledgements

This research was supported by 973 Project (No. 2012CB619102), the National Science and Technology Support Program (No. 2012BAI18B01) and the National Natural Science Foundation of China (No. 31370956) to Xi at Peking University, and the Rebecca Q. Morgan Foundation Grant and the Cornell University Jeffrey S. Lehman Fund for Scholarly Exchange with China to Chu at Cornell University.

Notes and references

[a] Center for Biomedical Materials and Tissue Engineering, Academy for Advanced Interdisciplinary Studies, Peking University, Beijing 100871, China.

[b] School of Materials Science and Engineering, University of Science and Technology Beijing, Beijing 100083, China.

[c] Shenzhen Research Institute, Peking University, Shenzhen 518055, China.

[d] Biomedical Engineering Program Cornell University, Ithaca, NY, USA 14853-4401.

Reference

1 B. Heublein, R. Rohde, V. Kaese, M. Niemeyer, W. Hartung and A. Haverich, *Heart*, 2003, **89**, 651.

2 R. Erbel, C. Di Mario, J. Bartunek, J. Bonnier, B. de Bruyne, F. R. Eberli, P. Erne, M. Haude, B. Heublein, M. Horrigan, C. Ilsley, D. Böse, J. Koolen, T. F. Lüscher, N. Weissman and R. Waksman, *The Lancet*, 2007, **369**, 1869.

3 F. Witte, J. Fischer, J. Nellesen, H. -A. Crostack, V. Kaese, A. Pisch, F. Beckmann and H. Windhagen, *Biomaterials*, 2006, **27**, 1013.

4 M. P. Staiger, A. M. Pietak, J. Huadmai and G. Dias, *Biomaterials*, 2006, **27**, 1728.

5 C. H. Ye, Y. F. Zheng, S. Q. Wang, T. F. Xi and Y. D. Li, *Applied surface science*, 2012, **258**, 3420.

6 V. Kaesel, P. T. Tai, Fr. W. Bach, H. Haferkamp, F. Witte and H. Windhagen, *Magnesium: Proceedings of the 6th International Conference Magnesium Alloys and Their Applications*, 2004, 534.

7 N. Hort, Y. Huang, D. Fechner, M. Störmer, C. Blawert, F. Witte, C. Vogt, H. Drücker, R. Willumeit, K.U. Kainer and F. Feyerabend, *Acta Biomater*, 2010, **6**, 1714.

8 H. Hornberger, S. Virtanen and A. R. Boccaccini, *Acta Biomater*, 2012, **8**, 2442.

9 C. Blawert, W. Dietzel, E. Ghali and G. L. Song, *Advanced Engineering Materials*, 2006, **8**, 511.

10 M. Abulsain, A. Berkani, F. A. Bonilla, Y. Liu, M. A. Arenas, P. Skeldon, G. E. Thompson, P. Bailey, T. C. Q. Noakes, K. Shimizu and H. Habazaki, *Electrochimica Acta*, 2004, **49**, 899.

11 Y. Q. Chen, G. J. Wan, J. Wang, S. Zhao, Y. C. Zhao and N. Huang, *Corrosion Science*, 2013, **75**, 280.

12 M. D. Pereda, C. Alonso, L. Burgos-Asperilla, J. A. del Valle, O. A. Ruano, P. Perez and M. A. Fernández Lorenzo de Mele, *Acta Biomater*, 2010, **6**, 1772.

13 X. -L. Wang, N. Haraikawa, and S. Suda, *Journal of Alloys and Compounds*, 1995, **231**, 397.

14 T. T. Yan, L. L. Tan, D. S. Xiong, X. J. Liu, B. C. Zhang and K. Yang, *Materials Science and Engineering: C*, 2010, **30**, 740.

15 M. S. Killian, V. Wagener, P. Schmuki and S. Virtanen, *Langmuir*, 2010, **26**, 12044.

16 X. Liu, Z. L. Yue, T. Romeo, J. Weber, T. Scheuermann, S. Moulton and G. Wallace, *Acta Biomater*, 2013, **9**, 8671.

17 R. Pinto, M. J. Carmezim, M. G. S. Ferreira and M. F. Montemor, *Progress in Organic Coatings*, 2010, **69**, 143.

18 G. J. Wan, M. F. Maitz, H. Sun, P. P. Li and N. Huang, *Surface and Coatings Technology*, 2007, **201**, 8267.

19 X. M. Wang, X. Q. Zeng, G. S. Wu, S. S. Yao and Y. J. Lai, *J Alloy Compd*, 2007, **437**, 87.

20 C. L. Liu, Y. C. Xin, X. B. Tian and P. K. Chu, *Thin Solid Films*, 2007, **516**, 422.

21 J. X. Yang, F. Z. Zhang, I. -S. Lee, Q. S. Yin, H. Xia and S. X. Yang, *J Biomater Appl*, 2011, **27**, 153.

22 G. S. Wu, K. J. Ding, X. Q. Zeng, X. M. Wang and S. S. Yao, *Scripta Mater*, 2009, **61**, 269.
23 N. Yamauchi, N. Ueda, A. Okamoto, T. Sone, M. Tsujikawa and S. Oki, *Surface and Coatings Technology*, 2007, **201**, 4913.
24 M. E. Roy, L. A. Whiteside, J. Xu and B. J. Katerberg, *Acta Biomater*, 2010, **6**, 1619.
25 G. K. Jain, S. A. Pathan, S. Akhter, N. Ahmad, N. Jain, S. Talegaonkar, R. K. Khar and F. J. Ahmad, *Polymer Degradation and Stability*, 2010, **95**, 2360.
26 F. Long Mi, Y. M. Lin, Y. -B. Wu, S. S. Shyu and Y. -H. Tsai, *Biomaterials*, 2002, **23**, 3257.
27 K. G. Janoria and A. K. Mitra, *International journal of pharmaceutics*, 2007, **338**, 133.
28 W. Y. Chan, K. S. Chian and M. J. Tan, *Materials science & engineering. C, Materials for biological applications*, 2013, **33**, 5019.
29 Z. Y. Qian, S. Li, Y. He, H. L. Zhang and X. Liu, *Biomaterials*, 2004, **25**, 1975.
30 K. E. Uhrich, S. M. Cannizzaro, R. S. Langer and K. M. Shakesheff, *Chemical Reviews*, 1999, **99**, 3181.
31 A. C. Albertsson and I. K. Varma, *Biomacromolecules*, 2003, **4**, 1466.
32 N. Wang, X. S. Wu, C. Li and M. F. Feng, *Journal of Biomaterials Science, Polymer Edition*, 2000, **11**, 301.
33 X. H. Xu, P. Lu, M. Q. Guo and M. Z. Fang, *Applied surface science*, 2010, **256**, 2367.
34 C. L. Zhao, S. X. Zhang, C. H. He, J. N Li, B. L. Zhang and X. N. Zhang, *Journal of Functional Materials*, 2008, **39**, 987.(in Chinese)
35 J. N. Li, P. Cao, X. N. Zhang, S. X. Zhang and Y. H. He, *Journal of Materials Science*, 2010, **45**, 6038.
36 J. J. Huang, Y. B. Ren, B. C. Zhang and K. Yang, *Transactions of Nonferrous Metals Society of China*, 2007, **17**, 1465. (in Chinese)
37 S. Lyu, R. Sparer and D. Untereker, *Journal of Polymer Science Part B: Polymer Physics*, 2005, **43**, 383.
38 K. M. DeFife, K. Grako, G. Cruz-Aranda, S. Price, R. Chantung, K. Macpherson, R. Khoshabeh, S. Gopalan and W. G. Turnell, *J Biomater Sci Polym Ed*, 2009, **20**, 1495.
39 S. H. Lee, I. Szinai, K. Carpenter, R. Katsarava, G. Jokhadze, C. C. Chu, Y. M. Huang, E. Verbeken, O. Bramwell, I. De Scheerder and M. K. Hong, *Coron Artery Dis*, 2002, **13**, 237.
40 C. C. Chu, D. R. Fischell and M. Pomerantz, *9th World Biomaterials Congress*, 2012.
41 H. T. Cui, Y. D. Liu, M. X. Deng, X. Pang, P. B. Zhang, X. H. Wang, X. S. Chen, Y. Wei and X. S. Chen, *Biomacromolecules*, 2012, **13**, 2881.
42 X. Pang and C. C. Chu, *Biomaterials*, 2010, **31**, 3745.
43 X. Pang, J. Wu, C. Reinhart-King and C. C. Chu, *J. Polym. Sci. Part A: Polym. Chem.*, 2010, **48**, 3758.
44 J. Wu, D. Q. Wu, M. A. Mutschler and C. C. Chu, *Advanced Functional Materials*, 2012, **22**, 3815.
45 M. Y. He, A. Potuck, Y. Zhang and C. C. Chu, *Acta Biomaterialia*, 2014, **10**, 2482.
46 J. Wu, D. Yamanouchi, B. Liu and C. C. Chu, *J Mater Chem Lett*, 2012, **22**, 18983.
47 J. Wu, M. A. Mutschler and C. C. Chu, *J Mater Sci Mater Med*, 2011, **22**, 469.
48 D. Yamanouchi, J. Wu, A. N. Lazar, K. C. Kent, C. C. Chu and B. Liu, *Biomaterials*, 2008, **29**, 3269.
49 S. D. Suzanne Schwartz, C. C. Chu, J. White, A. Cooper, M. Rothrock, M. Adelman and R. Yurt, *3rd World Union of Wound Healing Societies*, 2008.
50 C. C. Chu*, J Fiber Bioengineering and Informatics*, 2012, **5**, 1.
51 C. C. Chu and R. Katsarava, *US Patent* 2003, No 6503538.
52 S. H. M. Webster, D. McClean, W. Jaffe, J. Ormiston, A. Aitken, T. Watson, *Euro Intervention*, 2013, **9**, 46.
53 K. Guo and C. C. Chu, *J. Appl. Polym*, 2008, **110**, 1858.
54 K. Guo and C. C. Chu, *J. Biomater.* , 2007, **18**, 489.
55 E. Chkhaidze, D. Tugushi, D. KharadzE, Z. Gomurashvili, C. C. Chu and R. Katsarava, *Journal of Macromolecular Science, Part A: Pure and Applied Chemistry*, 2011, **48**, 544.
56 L. Li and C. C. Chu, *J. Biomater. Sci. Polym. Ed.*, 2009, **20**, 341.
57 D. Q. Wu, J. Wu and C. C. Chu, *Soft Matter*, 2013, **9**, 3965.
58 K. Guo and C. C. Chu, *J Polym Sci Polym Chem Ed*, 2007, **45**, 1595.
59 G. Jokhadze, M. Mschaidze, H. Panosyan, C. C. Chu and R. Katsarava, *J. Biomater. Sci. Polymer Edn*, 2007, **18**, 411.
60 J. A. Horwitz, K. M. Shum, J. C. Bodle, M. Deng, C. C. Chu and C. A. Reinhart-King, *Journal of biomedical materials research. Part A*, 2010, **95**, 371.
61 M. X. Deng, J. Wu, C. A. Reinhart-King and C. C. Chu, *Acta Biomaterialia*, 2011, **7,** 1504.
62 W. M. De, Z. X. Wang, K. M. Atkins, K. Mequanint and E. R. Gillies, *J. Polym. Sci. part A: Polym. Chem*, 2008, **46**, 6376.
63 D. Q. Wu, X. H. Qin and C. C. Chu, *9th World Biomaterials Congress*, 2012.
64 J. W and C. C. Chu, *J. Mater. Chem. B*, 2013, **1**, 353.
65 M. X. Deng, J. Wu, C. A. Reinhart-King and C. C. Chu, *Biomacromolecules*, 2009, **10**, 14.
66 A. Rodríguez-Galán, L. Fuentes and J. Puiggalí, *Polymer*, 2000, **41**, 5967.
67 K. DeFife, S. Gopalan, S. Price, G. Cruz-Aranda, R. Chantung and W. Turnell, *30th Annual Meeting of the Society for Biomaterials*, 2005.
68 L. Xu and A. Yamamoto, *Colloids and surfaces. B, Biointerfaces*, 2012, **93**, 67.
69 A. Mandelli, M. Bestetti, A. Da Forno, N. Lecis, S. P. Trasatti and M. Trueba, *Surface and Coatings Technology*, 2011, **205**, 4459.
70 X. N. Gu, N. Li, W. R. Zhou, Y. F. Zheng, X. Zhao, Q. Z. Cai and L. Ruan, *Acta Biomater*, 2011, **7**, 1880.
71 L. Yang and E. Zhang, *Materials Science and Engineering C*, 2009, **29**, 1691.
72 A. C. Hänzi, P. Gunde, M. Schinhammer and P.J. Uggowitzer, *Acta Biomaterialia*, 2009, **5**,162.
73 X. N. Gu, N. Li, Y. F. Zheng and L. Ruan, *Materials Science and Engineering B*, 2011, **176**, 1778.
74 A. Abdal-hay, M. Dewidar and J. K. Lim, *Applied surface science*, 2012, **261**, 536.
75 N. J. Ostrowski, B. Lee, A. Roy, M. Ramanathan and P. N. Kumta, *J Mater Sci Mater Med*, 2013, **24**, 85.
76 W. Tang, X. Weng, L. Deng, K. Xu and J. Lu, *Surface and Coatings Technology*, 2007, **201**, 5664.
77 P. Lu, Y. Liu, M. Guo, H. Fang and X. Xu, *Materials Science and Engineering: C*, 2011, **31**, 1285.

78 R. Arrabal, E. Matykina, F. Viejo, P. Skeldon and G. E. Thompson, *Corrosion Science*, 2008, **50**, 1744.
79 T. S. N. Sankara Narayanan, I. S. Park and M. H. Lee, *Journal of Materials Chemistry B*, 2014, **2**, 3365.
80 H. Ardelean, I. Frateur and P. Marcus, *Corrosion Science*, 2008, **50**, 1907.
81 C. N. Cao, Principles of Electrochemistry of Corrosion, 2008, 139.(in Chinese)
82 G. Baril and N. Pébère, *Corrosion Science*, 2001, **43**, 471.
83 M. C. Zhao, M. Liu, G. L. Song and A. Atrens, *Corrosion Science*, 2008, **50**, 3168.
84 N. Pebere, C. Riera and F. Dabosi, *Electrochimica Acta*, 1990, **35**, 555.
85 G. Song, A. Atrens, X. Wu and B. Zhang, *Corrosion Science*, 1998, **40**, 1769.
86 E. M. Sherif and A. A. Almajid, *Int. J. Electrochem. Sci.*, 2011, **6**, 2131.
87 T. F. da Conceicao, N. Scharnagl, C. Blawert, W. Dietzel and K. U. Kainer, *Thin Solid Films*, 2010, **518**, 5209.
88 Y. L. Cheng, T. W. Qin, H. M. Wang and Z. Zhang, *Transactions of Nonferrous Metals Society of China*, 2009, **19**, 517.
89 W. R. Zhou, Y. F. Zheng, M. A. Leeflang and J. Zhou, *Acta Biomater,* 2013, **9**, 8488.
90 X. Lin, X. Yang, L. Tan, M. Li, X. Wang, Y. Zhang, K. Yang, Z. Hu and J. Qiu, *Applied surface science*, 2014, **288**, 718-726.
91 L. Xu and A. Yamamoto, *Applied surface science*, 2012, **258**, 6353.
92 B. Hadzima, M. Mhaede and F. Pastorek, *Journal of Materials Science: Materials in Medicine*, 2014, **25**, 1227.
93 F. Witte, V. Kaese, H. Haferkamp, E. Switzer, A. Meyer-Lindenberg, C. J. Wirth and H. Windhagen, *Biomaterials*, 2005, **26**, 3557.
94 J. Zhou, X. Zhang, Q. Li, Y. Liu, F. Chen and L. Li, *Journal of Materials Chemistry B*, 2013, **1**, 6213.
95 C. H. Kum, Y. Cho, Y. K. Joung, J. Choi, K. Park, S. H. Seo, Y. S. Park, D. J. Ahn and D. K. Han, *Journal of Materials Chemistry B*, 2013, **1**, 2764.
96 L. Li, J. Gao and Y. Wang, *Surface and Coatings Technology*, 2004, **185**, 92.
97 Y. Chen, Y. Song, S. Zhang, J. Li, C. Zhao and X. Zhang, *Biomed Mater*, 2011, **6**, 025005.
98 N. Ostrowski, B. Lee, N. Enick, B. Carlson, S. Kunjukunju, A. Roy and P. N. Kumta, *Acta Biomaterialia*, 2013, **9**, 8704.
99 K. Cai, A. Rechtenbach, J. Y. Hao, J. Bossert and K. D. Jandt, *Biomaterials*, 2005, **26**, 5960.
100 R. Rajaraman, D. E. Rounds, S. P. S. Yen and A. Rembaum, *Experimental Cell Research*, 1974, **88**, 327.
101 C. Wu, J. Chang, J. Wang, S. Ni and W. Zhai, *Biomaterials*, 2005, **26**, 2925.
102 W. Chen, T. Long, Y. J. Guo, Z. A. Zhu and Y. P. Guo, *Journal of Materials Chemistry B*, 2014, **2**, 1653.
103 X. Wang, X. Chen, L. Xing, C. Mao, H. Yu and J. Shen, *Journal of Materials Chemistry B*, 2013, **1**, 5036.
104 N. Kong, K. Lin, H. Li and J. Chang, *Journal of Materials Chemistry B*, 2014, **2**, 1100.
105 T. Nakaki, M. Nakayama and R. Kato, *European Journal of Pharmacology: Molecular Pharmacology*, 1990, **189**, 347.
106 F. C. Tanner, P. Meier and H. Greute, *Circulation*, 2000, **101**, 1982.
107 T. L. Cornwell, E. Arnold and N. J. Boerth, T. M. Lincoln, *Am J Physiol*, 1994, **267**, 1405.

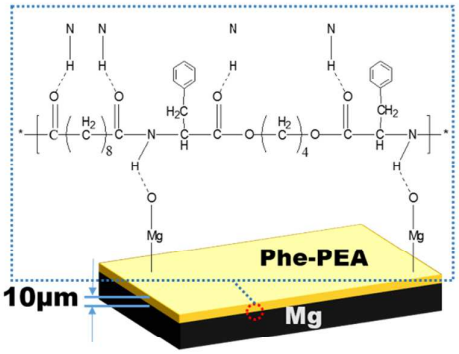

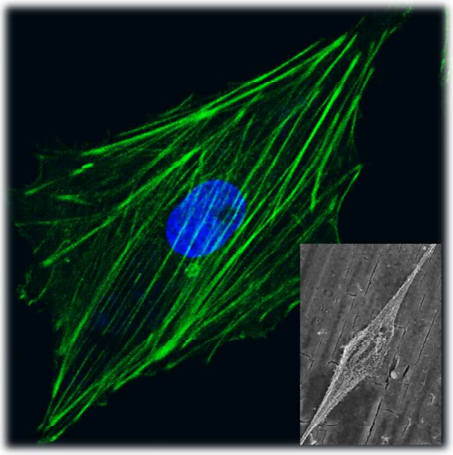

30 days
immersion
Surface
degradation